Contents lists available at *Dergipark*

Journal of Scientific Reports-A

journal homepage: *https://dergipark.org.tr/tr/pub/jsr-a*

E-ISSN: 2687-6167 ***Number 58, September 2024***

RESEARCH ARTICLE

Receive Date: 24.06.2024 *Accepted Date: 29.07.2024*

Assessments of GPS satellite orbiting period effects on diurnal and semi-diurnal luni-solar declinations utilizing Galileo satellites

Huseyin Duman[a,*]

[a] *Sivas Cumhuriyet University, Departments of Geomatics Engineering, 58140 Sivas, Türkiye, ORCID: 0000-0002-7340-7800*

Abstract

Global Navigation Satellite Systems (GNSS) can observe a variety of surface deformations on Earth, including periodic oscillations at different frequencies. An example of such phenomena is ocean tide loadings (OTL), which result from the redistribution of water mass. The Global Positioning System (GPS) exhibits orbital geometry that causes its revisit and orbital periods to coincide with the diurnal and semi-diurnal luni-solar declination constituents, known as K1 and K2, respectively. Consequently, the system faces challenges in accurately estimating these periodic oscillations due to its orbital artifacts. This study aims to quantify the extent to which GPS orbital artifacts introduce periodic signals into the K1 and K2 constituents by utilizing the Galileo system and determining the most suitable positioning approach. A dataset from the International GNSS Service (IGS), spanning 40 days in 2024 and covering six stations, was analyzed. Coordinates were estimated using both kinematic positioning every 5 minutes and a 6-hour static precise point positioning (PPP) mode with a 3-hour shift. The power spectra for the east, north, and up components indicated that, on average, the GPS system contributes 52.8% to the K1 constituents and 66.3% to the K2 constituents. Despite expectations that the diurnal K1 and semi-diurnal K2 tidal constituents would be more prominent in the power spectra of the GPS comparing to that of natural signature or of other navigation system (Galileo for this study), the diurnal K1 tidal constituent appeared weak in the kinematic mode power spectra for the GPS system. These findings validate that the overlapped-static PPP mode is a more appropriate approach for estimating these periodic deformations.

Keywords: GPS; Galileo; Power-spectra; Tidal Loadings; PPP

1. Introduction

The gravitational interactions between the Sun, the Moon, and the Earth induce periodic oscillations on the Earth's surface, manifesting as both solid Earth tides and ocean tides.

These ocean tides cause deformations on the Earth's surface due to the periodic redistribution of water mass, a phenomenon known as ocean tide loadings (OTL) [1]. The OTL deformations are responsive to geodetic measurements such as Global Navigation Satellite Systems (GNSS), Very Long Baseline Interferometry (VLBI), Satellite Laser Ranging (SLR), Doppler Orbitography Integrated by Satellite (DORIS) [2], which means these deformations could also be measurable by the geodetic techniques. However, among the GNSS systems, Global Positioning System (GPS) has a disadvantage of observing diurnal (K1 ~11.97 hours [3]) and semi-diurnal (K2 ~23.93 hours [3]) luni-solar declinations constituents because of aligning these constituents with the GPS revisit period and orbital period [4], [5], [6], although it provides more precise positioning estimates than the other geodetic techniques.

The problematic K1 and K2 luni-solar declination constituents, influenced by the GPS orbital geometry, have been measured more accurately by incorporating other Global Navigation Satellite Systems (GNSS) such as Global'naya Navigatsionnaya Sputnikovaya Sistema (GLONASS) and Galileo [1], [2], [6]. Abbaszadeh et al. [2] utilized the GLONASS system and reported that estimates for all OTL constituents, except K1 and K2, were as precise as those using the GPS system. However, the estimates for K1 and K2 showed improvement when compared to GPS alone. Ait-Lakbir et al. [6] demonstrated that the Galileo and/or GLONASS systems enhanced K1 and K2 estimates by up to 55% compared to GPS. Matviichuk et al. [1] indicated that K1 and K2 estimates are more accurate using GPS+GLONASS for the north and up topocentric coordinate components, whereas the GPS positioning with resolved ambiguities yielded better estimates for the east component than the combined solution. Peng et al. [5], rather than using coordinate time series, examined multi-GNSS interferometric reflectometry to analyze tidal constituents. They found that the bias on the K1 and K2 constituents due to GPS could be reduced by incorporating the Galileo and GLONASS systems. Furthermore, Pan et al. [7] proposed a novel methodology to accurately estimate the problematic K1 and K2 constituents using only the GPS system. This methodology involves fitting a quadratic smooth function to the tidal constituents, benefiting from the unique orbital geometry of other satellite systems in comparison to GPS. Wang et al. [8] benefitted from GPS, GLONASS, Galileo navigation satellites and their combinations to improve ocean tide loading estimates and highlighted that Galileo-only solution and multi-GNSS combinations showed better estimation of solar-related tidal constituents, specifically for K1 and K2 tidals, than GPS-only solutions. Additionally, they stated that resolving ambiguities is a vital role to estimate solar-related tidal constituents.

The studies [1], [2], [6], [9] predominantly processed their observation data using coordinate time series in precise point positioning (PPP) mode [10]. The commonly adopted PPP mode is a kinematic approach. Matviichuk et al. [1] estimated coordinates every 5 minutes in kinematic PPP mode, while Abbaszadeh et al. [2] used kinematic PPP mode with float ambiguities, as described by Penna et al. [11]. Ait-Lakbir et al. [6] processed data in both kinematic and non-overlapping 3-hour static PPP modes, finding the latter more reliable for estimating OTL displacements. Wang et al. [8] also reported similar findings with Ait-Lakbir et al. [6] in terms of data processing strategy. Bogusz and Figurski [9] employed a 3-hour static mode with a 1-hour shift, creating a 2-hour overlapping window, to analyze short-term OTL displacements.

The aforementioned studies primarily concentrate on the precise estimation of K1 and K2 tidal constituents due to the GPS orbital geometry, rather than on the artificial signal contributions to natural phenomena. This paper addresses two key objectives: (i) evaluating the extent to which the signal powers of the diurnal (K1) and semi-diurnal (K2) luni-solar declinations, which coincide with GPS revisit and orbital periods, are contaminated or interfered with by artificial signals induced by GPS orbital geometry; and (ii) determining which PPP mode—kinematic or overlapped-static PPP—is more effective in identifying these artificial signals attributed to GPS orbits. The structure of this paper is as follows. The details of the GNSS data and processing methodologies are elaborated in the following section. Section 3 outlines the preliminary analysis of coordinate time series, including outlier detection and precision assessment, and the transformation of these time series into the frequency domain. Finally, the key findings addressing the research questions are highlighted in the concluding section.

2. GNSS Data Acquisition and Processing

GNSS data from six IGS stations distributed across the Eastern Mediterranean region were employed in this study (Fig. 1). The data were obtained from the online archives of the Crustal Dynamics Data Information System

(CDDIS) (https://cddis.nasa.gov, last accessed: April 7, 2024) in the daily Receiver Independent Exchange (RINEX v3) in Hatanaka format sampled at every 30-seconds [12]. These stations fully include 40 days of data covering January 1, 2024, to February 9, 2024.

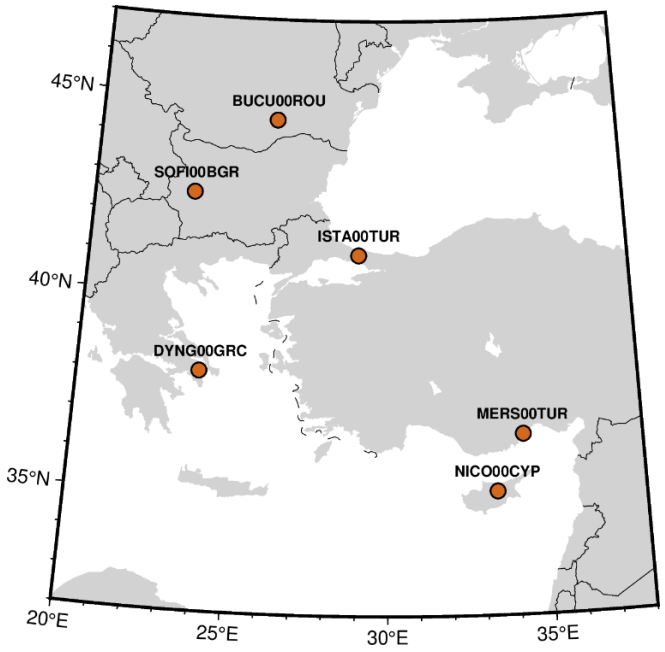

Fig. 1. The six stations operated under the International GNSS Service (IGS) with long name convention.

The PRIDE-PPPAR v3.0 software were utilized to process all 40 days of daily RINEX observation files [13], with processing parameters outlined in Table 1. Coordinates were estimated in both static and kinematic Precise Point Positioning (PPP) modes [10], resolving ambiguities for GPS- and Galileo-only observations [14], [15], [16]. The static PPP strategy entailed a 6-hour session length with a 3-hour session overlap (Fig. 2), while kinematic PPP coordinates were estimated every 300 seconds using non-overlapping observations.

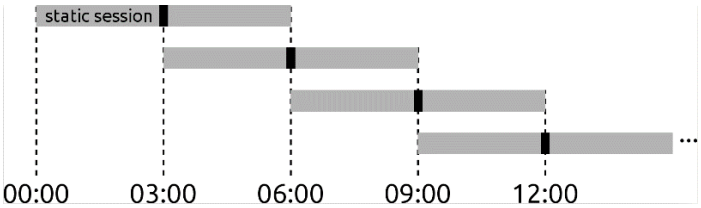

Fig. 2. A 3-hours overlapped 6-hours length static session strategy.

Rapid orbit/clock products, satellite attitude quaternions, observable-specific phase biases, and Earth rotation parameters from Wuhan University were utilized in all processing [15], [17], [18]. The quality of parameter estimates using rapid products has been previously reported by Li et al. [19], showing comparability with final products. Second-order ionospheric effects were mitigated using CODE products [20]. Vienna Mapping Function (VMF1) data were applied [21], with zenith wet delays estimated using a random-walk model, and gradients for horizontal delays estimated using a piece-wise constant model every 12 hours. Pole and Solid Earth tides were accounted for according to International Earth Rotation Service (IERS) conventions [22]; however, ocean tide loadings were not modeled. The GNSS stations in Fig. 1 are far from oceanic boundaries. Even so, they have too

small signal amplitudes for K1 and K2 constituents, this omission was due to clearly exhibiting how much power of the GPS orbital revolution periods adds to the diurnal, semi-diurnal luni-solar declinations (K1 and K2) constituents.

Table 1. PPP processing details for GNSS data

Parameter	Description
Software	PRIDE-PPPAR v3.0
Positioning Strategy	PPP in overlapped-static and kinematic mode. Ionosphere-free combinations for code and phase with every 30 seconds in static mode and every 300 seconds in kinematic mode
Elevation cut-off angle	7^o
Products	Wuhan University rapid products (WUM): Earth rotation parameters, observable-specific phase biases, satellite attitude Quaternions, orbit and clock products
Phase Center of Satellite/Receiver	IGS20_2290.atx
Phase Ambiguities	Fixing GPS and Galileo satellites above 15^o cut-off angle and 15-min arc length
Ionosphere	Removed second order effect using CODE products
Troposphere	VMF1
Zenit wet delays	Random-walk
Gradients of horizontal delays	Piece-wise constant at evert 12 hours
Ocean tide loading	Not modelled
Solid earth and pole tides	IERS conventions 2010

3. Results and Discussion

This section presents: (i) a 40-day time series of coordinates for all stations using GPS- and Galileo-only systems in both overlapped static (Fig. 2) and kinematic PPP modes, and (ii) stacked spectra for the east (E), north (N), and up (U) coordinate components in the frequency domain (with frequencies converted to periods) using the Lomb-Scargle algorithm [23], [24]. The analysis evaluates the contribution of the GPS orbiting period to diurnal (K1) and semi-diurnal (K2) luni-solar declinations constituents and compares the efficiency of overlapped static and kinematic positioning strategies.

3.1. GPS- and Galileo-only systems coordinate time series

The three-dimensional cartesian coordinates of the six selected stations aligned to the ITRF2020 reference frame [25] were transformed into the topocentric coordinate system (i.e., east, north, and up), using the average coordinates over the 40-day period as a reference. These averaged reference coordinates were generated using similar processing parameters as detailed in the previous section (see Table 1) but employing a non-overlapped 24-hour session strategy in static PPP mode for both GPS- and Galileo-only system observations.

Outliers in the kinematic and overlapped-static time series for the topocentric coordinate components were removed through median absolute deviation (MAD) method [26], [27], [28], which is of the form:

$$MAD = \begin{cases} \frac{1.2533}{N} \times \sum |\boldsymbol{e}|, & median(|\boldsymbol{e}|) = 0 \\ 1.4826 \times median(|\boldsymbol{e}|), & median(|\boldsymbol{e}|) \neq 0 \end{cases} \quad (1)$$

where, $|\cdot|$ is the absolute operator, and $\boldsymbol{e} = \boldsymbol{y} - median(\boldsymbol{y})$ is normalized observations referencing to the median of observations or observations residuals. N is the number of observations. Any residuals in $|\boldsymbol{e}|$ exceeding $3 \times MAD$ threshold is considered as outliers and removed from the time series.

The analysis results, e.g., the north component of the DYNG00GRC station using GPS- and Galileo-only systems in kinematic and overlapped-static PPP modes (Fig. 3), provide valuable insights into the comparative performance of GPS and Galileo satellite systems. After removing outliers from the coordinate time series (gray solid lines for kinematic mode and black crosses for overlapped-static mode in Fig. 3), the kinematic coordinates align well with the static coordinates. Table 2 presents the outlier percentages and root mean square error (RMSE) comparisons for the east, north (horizontal), and up components. The outlier percentages for kinematic coordinate time series range from 1.40% to 4.41% for GPS and from 1.76% to 4.66% for Galileo, except for the ISTA00TUR station. For this station, the percentages reach up to 15.82% and 45.25% for GPS and Galileo, respectively. The RMSE values for kinematic coordinate time series for GPS vary between 5.00 mm and 9.77 mm for horizontal components and between 16.72 mm and 24.90 mm for vertical components, whereas those for Galileo range from 5.85 mm to 9.98 mm for horizontal components and from 18.58 mm to 47.93 mm for the vertical component. Although the ISTA00TUR station has a high percentage of outliers, its RMSE values are comparable to those of other stations. For the static coordinate time series, both the outlier percentages and RMSE values are generally lower compared to the kinematic time series. The outlier percentages range from 0.00% to 9.43% for GPS and from 0.31% to 14.78% for Galileo. These upper values correspond to the horizontal components of the DYNG00GRC and SOFI00BGR stations and are higher than their kinematic counterparts. The RMSE values for GPS range between 1.59 mm and 2.72 mm for horizontal components, and between 5.98 mm and 12.48 mm for the vertical component. For Galileo, the RMSE values range from 1.74 mm to 2.80 mm for horizontal components and from 6.76 mm to 12.38 mm for the vertical component. The RMSE values for GPS and Galileo across all components are quite close to each other.

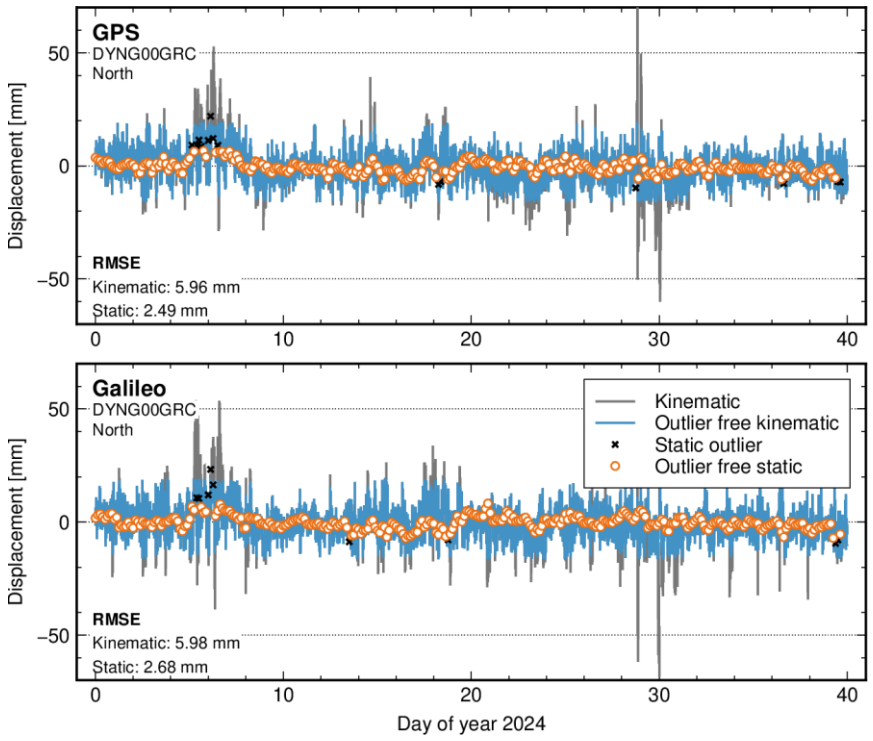

Fig. 3. The north component displacements of station DYNG00GRC, comparing kinematic and static positioning modes with GPS (top) and Galileo (bottom) satellites. The gray solid line represents raw displacements in kinematic positioning, while the blue solid line depicts the same with outliers removed. In static mode, outliers are denoted by black crosses, whereas outlier-free static mode displacements are indicated by orange outlined circles.

Table 2. Outlier percentage and RMSE comparison of east (E), north (N) and up (U) components for kinematic and static positioning modes with GPS and Galileo satellites

Stations	Outliers [%]		RMSE* [mm]	
	Kinematic-mode	Static-mode	Kinematic-mode	Static-mode
	E / N / U		E / N / U	
			GPS	
BUCU00ROU	2.34 / 1.48 / 1.37	1.89 / 0.63 / 0.31	5.17 / 7.27 / 16.92	2.24 / 1.59 / 8.41
DYNG00GRC	4.41 / 3.54 / 2.88	7.23 / 4.40 / 1.89	5.00 / **5.96**$^{+}$ / 16.72	2.29 / **2.49**$^{+}$ / 6.75
ISTA00TUR	15.82 / 11.87 / 9.83	0.95 / 0.95 / 0.32	6.21 / 7.85 / 20.80	2.12 / 1.94 / 6.97
MERS00TUR	1.61 / 2.01 / 1.47	1.57 / 0.00 / 0.63	6.21 / 8.43 / 21.17	1.95 / 2.00 / 6.97
NICO00CYP	1.93 / 2.60 / 1.40	0.00 / 0.00 / 0.94	5.41 / 7.23 / 21.92	2.00 / 1.95 / 5.98
SOFI00BGR	2.77 / 1.92 / 1.85	9.43 / 3.14 / 1.57	8.63 / 9.77 / 24.90	2.72 / 2.35 / 12.48
			Galileo	
BUCU00ROU	2.22 / 1.76 / 1.60	3.46 / 0.94 / 1.26	5.97 / 6.71 / 18.58	2.18 / 1.74 / 9.27
DYNG00GRC	3.58 / 3.94 / 3.01	5.03 / 2.83 / 2.20	5.85 / **5.98**$^{+}$ / 19.64	2.70 / **2.68**$^{+}$ / 7.51
ISTA00TUR	45.25 / 35.24 / 32.65	3.47 / 0.95 / 0.63	8.56 / 12.65 / 47.93	2.30 / 2.20 / 8.35
MERS00TUR	3.46 / 2.63 / 2.68	0.94 / 0.31 / 2.20	6.93 / 7.71 / 24.74	2.49 / 2.22 / 6.97
NICO00CYP	4.66 / 4.03 / 3.68	2.52 / 1.26 / 0.94	6.19 / 6.93 / 24.81	2.20 / 1.98 / 6.76
SOFI00BGR	3.84 / 2.70 / 2.58	14.78 / 4.40 / 1.26	8.88 / 9.98 / 27.29	2.52 / 2.80 / 12.38

* RMSE is computed using outlier-free time series

$^{+}$ These values are depicted in Fig. 3

3.2. Stacked spectra for GPS- and Galileo-only systems

The PPP coordinate time series for GPS- and Galileo-only systems in kinematic and overlapped-static mode elaborated in the previous section are used to examine the GPS system specific orbital period effects on luni-solar declinations. The orbital period equals to $11^{h}\ 58^{m}$, which resulting in two orbital repeats in one sidereal day. This amounts to a 1:2 deep resonant effect on GPS satellites relative to the Earth's rotation [4], [29]. The main luni-solar declinations, i.e., K1 and K2 equivalent either to one sidereal day and its half, coincidence with the GPS orbital period [5]. It means that the signal powers at K1 and K2 frequencies are contaminated by the GPS orbital error, so leading to hinder the detectable natural signature of these frequencies. However, Galileo satellite system has rather a 10:17 shallow resonant effect relative to the Earth's rotation [29]. It means that the Galileo system specific orbital error does not affect the signal powers at the K1 and K2 frequencies, that is, the expected signal powers at these frequencies when using coordinate time series derived only from Galileo system are their detectable natural signature.

To investigate the GPS orbital periodical effect, the coordinate time series for the topocentric coordinate components of all stations were transformed to the frequency domain through the Lomb-Scargle method [23], [24]. The power spectra were generated by stacking the power spectra of each station at equivalent frequencies and subsequently normalizing the powers. This process was performed separately for the east, north, and up components of the kinematic and overlapped-static time series derived from GPS and Galileo systems. Fig. 4 illustrates the corresponding power spectra converted to periods by inverting the frequencies. The K1 and K2 constituents are clearly visible in all components for the overlapped-static mode. For the kinematic mode, these constituents demonstrate a relatively weak presence in all components, except for the K2 in the east component, which shows nearly no signature. In addition to these signals, the 3rd and 4th harmonics of luni-solar declinations (K3 and K4) and the principal lunar semi-diurnal (M2) constituent also appear in the spectra. In the overlapped-static mode, the K3 harmonic has too weak signature in all components, whereas the K4 has no power. The sampling period of the overlapped-static mode is three hours. The Nyquist frequency of this three-hour interval limits the capability to detect the K3 and higher harmonics. The weak presence of K3 despite this limitation could originate from the overlapping strategy. Conversely, in the kinematic mode, these harmonics have distinctive features in the horizontal components, except for the up component due to the sampling interval. The sampling interval of the kinematic mode

(5 minutes) is shorter than that of the overlapped-static mode. The M2 constituent appears in the east and up components, yet it is absent in the north component for both positioning modes.

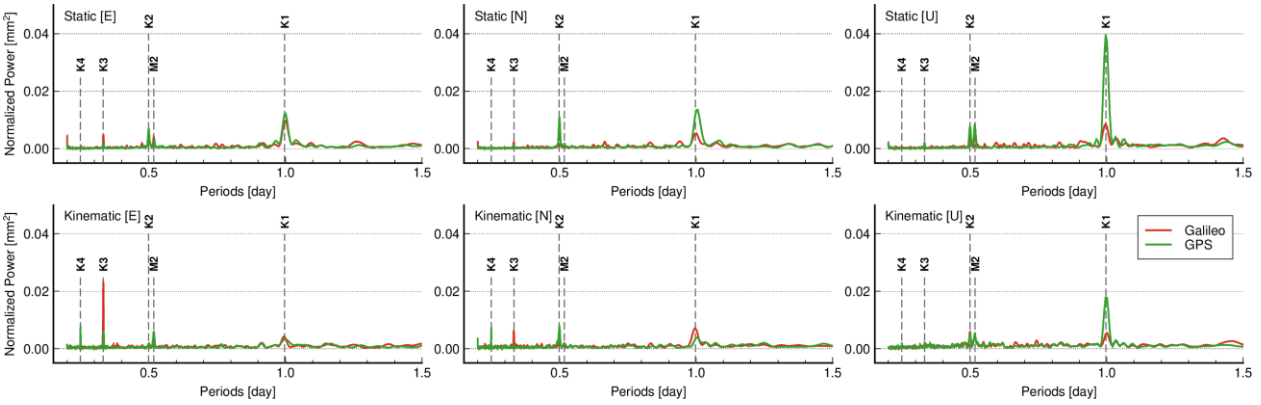

Fig. 4. East (E), north (N) and up (U) components stacked mean power spectra in kinematic and overlapped-static mode for GPS (solid green line) and Galileo (solid red line) satellites. The vertical dashed gray lines represent diurnal, semi-diurnal luni-solar declinations (K1 and K2) and harmonics (K3 and K4), and principal lunar semi-diurnal (M2) constituents.

The K1 and K2 constituents consist of a natural phenomenon of luni-solar declinations and the GPS orbital geometry for the spectra of GPS. But those for the spectra of Galileo include only the natural signature, there is not a system specific artificial error. Therefore, the signal power at the K1 and K2 constituents for GPS system should be higher than those for Galileo system. In the power spectra of the horizontal components for kinematic PPP mode, the signal power at K1 for the Galileo is higher than GPS, which is out of the stated expectation. It clearly implies that the overlapped-static PPP mode has a prior to the kinematic PPP mode.

A difference of the signal power at K1 and K2 between GPS and Galileo systems explains how much signal power is introduced in the natural phenomenon. Assuming the signal power of Galileo is equivalent that of the natural K1 and K2 signal powers, then the contribution of GPS system in percentage (ϕ) is of the form,

$$\phi = \left\{ \frac{P_{GPS}(c) - P_{GAL}(c)}{P_{GPS}(c)} \right\} \times 100\% \tag{2}$$

where, c is the K1 and K2 constituents; $P_{GPS}(c)$ and $P_{GAL}(c)$ are the signal powers at c frequency/period. Using the signal powers in Fig. 4, the GPS orbit periodical effect on the K1 constituents is 19.6%, 60.7% and 78.2% for east, north and up components, whereas that on the K2 constituents is 63.1%, 85.2% and 50.6% in similar order. The statistics show that the signal powers at the K1 and K2 constituents originate mostly from the GPS orbital periodic effect, except for the east component for the K1.

4. Conclusions

The GPS system orbital period coincides with the first two harmonics of lunar-solar declinations, known as K1 and K2. Consequently, a periodic signal resulting from the GPS satellite system's orbital geometry interferes with this natural phenomenon, rendering it undetectable through GPS-only observations. In contrast, the Galileo satellite system, despite its similarities to GPS, has a different orbital period, meaning it does not affect the lunar-solar declinations. This study quantifies the extent to how much the luni-solar declinations are contaminated or interfered with by the GPS satellite system's orbital period, using the Galileo satellite system for comparison. Additionally, the study evaluates the reliability of results produced by either the kinematic or overlapped-static PPP mode. The results demonstrate that the GPS system provides more precise coordinate estimates than the Galileo system by a factor of nearly 1.2. In kinematic PPP mode, the average root mean square errors (RMSE) for the horizontal components are

6.9 / 7.7 mm, and those for the vertical component are 20.4 / 27.2 mm for GPS and Galileo systems, respectively. In overlapped-static PPP mode, these values are significantly lower, and are 2.1 / 2.3 mm and 7.9 / 8.5 mm in similar order. The spectrum analysis reveals notable differences between the GPS and Galileo systems. Specifically, the GPS system exhibits artificial signals corresponding to its orbital period (K2) and revisit period (K1). These artificial signals are more prominent in the power spectra of the overlapped-static PPP mode, validating its superiority over the kinematic PPP mode in isolating GPS system-specific signals. The unexpected presence of the first harmonic of the luni-solar declination (K1) in the horizontal components' power spectra for the kinematic PPP mode further supports this finding. In contrast, assuming that the Galileo system's power spectra predominantly represent natural phenomena, with the artificial signals in the GPS system contributing on average 52.8% and 66.3% to the K1 and K2 periods, respectively. This significant impact of artificial signals induced by the GPS satellite system underscores the necessity for careful consideration in geophysical studies. Overall, this research highlights the advantages of the Galileo system in providing contribution of GPS orbital geometry error into luni-solar declinations and the effectiveness of the overlapped-static PPP mode in extracting these signals.

Acknowledgements

The Generic Mapping Tools (GMT) was utilized for all figures [30]. The GNSS data were retrieved from the online archives of the CDDIS repository. I extend my appreciation to the WUHAN University for supplying PRIDE PPP-AR II software and the precise orbit/clock products, and to the PRIDE PPP-AR software team for their ongoing dedication to enhancing the software.

Author Contribution

H.Duman: Data Collection, analysis of data and interpretation results, final manuscript preparation

References

[1] B. Matviichuk, M. King, and C. Watson, “Estimating ocean tide loading displacements with GPS and GLONASS,” *Solid Earth*, vol. 11, no. 5, pp. 1849–1863, Oct. 2020, doi: 10.5194/se-11-1849-2020.
[2] M. Abbaszadeh, P. J. Clarke, and N. T. Penna, “Benefits of combining GPS and GLONASS for measuring ocean tide loading displacement,” *J. Geod.*, vol. 94, no. 7, p. 63, Jul. 2020, doi: 10.1007/s00190-020-01393-5.
[3] N. T. Penna and M. P. Stewart, “Aliased tidal signatures in continuous GPS height time series,” *Geophys. Res. Lett.*, vol. 30, no. 23, p. 2003GL018828, Dec. 2003, doi: 10.1029/2003GL018828.
[4] R. Zajdel, K. Kazmierski, and K. Sośnica, “Orbital Artifacts in Multi□GNSS Precise Point Positioning Time Series,” *J. Geophys. Res. Solid Earth*, vol. 127, no. 2, p. e2021JB022994, Feb. 2022, doi: 10.1029/2021JB022994.
[5] D. Peng, Y. N. Lin, J.-C. Lee, H.-H. Su, and E. M. Hill, “Multi-constellation GNSS interferometric reflectometry for tidal analysis: mitigations for K1 and K2 biases due to GPS geometrical errors,” *J. Geod.*, vol. 98, no. 1, p. 5, Jan. 2024, doi: 10.1007/s00190-023-01812-3.
[6] H. Ait-Lakbir, A. Santamaría-Gómez, and F. Perosanz, “Assessment of sub-daily ocean tide loading errors and mitigation of their propagation in multi-GNSS position time series,” *GPS Solut.*, vol. 27, no. 3, p. 129, Jul. 2023, doi: 10.1007/s10291-023-01467-9.
[7] H. Pan, X. Xu, H. Zhang, T. Xu, and Z. Wei, “A Novel Method to Improve the Estimation of Ocean Tide Loading Displacements for K1 and K2 Components with GPS Observations,” *Remote Sens.*, vol. 15, no. 11, p. 2846, May 2023, doi: 10.3390/rs15112846.
[8] H. Wang, M. Li, N. Wei, S.-C. Han, and Q. Zhao, “Improved estimation of ocean tide loading displacements using multi-GNSS kinematic and static precise point positioning,” *GPS Solut.*, vol. 28, no. 1, p. 27, Jan. 2024, doi: 10.1007/s10291-023-01568-5.
[9] J. Bogusz and M. Figurski, “Residual K1 and K2 Oscillations in Precise GPS Solutions: Case Study,” *Artif. Satell.*, vol. 46, no. 2, Jan. 2011, doi: 10.2478/v10018-011-0012-4.
[10] J. F. Zumberge, M. B. Heflin, D. C. Jefferson, M. M. Watkins, and F. H. Webb, “Precise point positioning for the efficient and robust analysis of GPS data from large networks,” *J. Geophys. Res. Solid Earth*, vol. 102, no. B3, pp. 5005–5017, Mar. 1997, doi: 10.1029/96JB03860.
[11] N. T. Penna, P. J. Clarke, M. S. Bos, and T. F. Baker, “Ocean tide loading displacements in western Europe: 1. Validation of kinematic GPS estimates,” *J. Geophys. Res. Solid Earth*, vol. 120, no. 9, pp. 6523–6539, Sep. 2015, doi: 10.1002/2015JB011882.
[12] C. E. Noll, “The crustal dynamics data information system: A resource to support scientific analysis using space geodesy,” *Adv. Space Res.*, vol. 45, no. 12, pp. 1421–1440, Jun. 2010, doi: 10.1016/j.asr.2010.01.018.
[13] J. Geng *et al.*, “PRIDE PPP-AR: an open-source software for GPS PPP ambiguity resolution,” *GPS Solut.*, vol. 23, no. 4, p. 91, Oct. 2019, doi: 10.1007/s10291-019-0888-1.
[14] J. Geng and S. Mao, “Massive GNSS Network Analysis Without Baselines: Undifferenced Ambiguity Resolution,” *J. Geophys. Res. Solid Earth*, vol. 126, no. 10, p. e2020JB021558, Oct. 2021, doi: 10.1029/2020JB021558.
[15] J. Geng, Q. Wen, Q. Zhang, G. Li, and K. Zhang, “GNSS observable-specific phase biases for all-frequency PPP ambiguity resolution,” *J. Geod.*, vol. 96, no. 2, p. 11, Feb. 2022, doi: 10.1007/s00190-022-01602-3.

[16] J. Geng, X. Chen, Y. Pan, and Q. Zhao, "A modified phase clock/bias model to improve PPP ambiguity resolution at Wuhan University," *J. Geod.*, vol. 93, no. 10, pp. 2053–2067, Oct. 2019, doi: 10.1007/s00190-019-01301-6.
[17] J. Geng, S. Yang, and J. Guo, "Assessing IGS GPS/Galileo/BDS-2/BDS-3 phase bias products with PRIDE PPP-AR," *Satell. Navig.*, vol. 2, no. 1, p. 17, Dec. 2021, doi: 10.1186/s43020-021-00049-9.
[18] J. Geng, Q. Zhang, G. Li, J. Liu, and D. Liu, "Observable-specific phase biases of Wuhan multi-GNSS experiment analysis center's rapid satellite products," *Satell. Navig.*, vol. 3, no. 1, p. 23, Oct. 2022, doi: 10.1186/s43020-022-00084-0.
[19] W. Li, M. Kačmařík, and D. Kin, "Assessment of the Multi-GNSS PPP Performance Using Precise Products from the Wuhan Analysis Centre," in *Proceedings of conference GIS Ostrava 2021 Advances in Localization and Navigation*, Vysoká škola báňská - Technická univerzita Ostrava, 2021. doi: 10.31490/9788024845050-9.
[20] S. Kedar, G. A. Hajj, B. D. Wilson, and M. B. Heflin, "The effect of the second order GPS ionospheric correction on receiver positions," *Geophys. Res. Lett.*, vol. 30, no. 16, p. 2003GL017639, Aug. 2003, doi: 10.1029/2003GL017639.
[21] J. Boehm, A. Niell, P. Tregoning, and H. Schuh, "Global Mapping Function (GMF): A new empirical mapping function based on numerical weather model data," *Geophys. Res. Lett.*, vol. 33, no. 7, p. 2005GL025546, Apr. 2006, doi: 10.1029/2005GL025546.
[22] G. Petit and B. Luzum, "IERS conventions (2010)," 2010.
[23] N. R. Lomb, "Least-squares frequency analysis of unequally spaced data," *Astrophys. Space Sci.*, vol. 39, no. 2, pp. 447–462, Feb. 1976, doi: 10.1007/BF00648343.
[24] J. D. Scargle, "Studies in astronomical time series analysis. II - Statistical aspects of spectral analysis of unevenly spaced data," *Astrophys. J.*, vol. 263, p. 835, Dec. 1982, doi: 10.1086/160554.
[25] Z. Altamimi, P. Rebischung, X. Collilieux, L. Métivier, and K. Chanard, "ITRF2020: an augmented reference frame refining the modeling of nonlinear station motions," *J. Geod.*, vol. 97, no. 5, p. 47, May 2023, doi: 10.1007/s00190-023-01738-w.
[26] J. W. Tukey, *Exploratory data analysis*. in Addison-Wesley series in behavioral science. Reading (Mass.) Menlo Park (Calif.) London [etc.]: Addison-Wesley publ, 1977.
[27] R. A. Maronna, R. D. Martin, and V. J. Yohai, *Robust Statistics: Theory and Methods*, 1st ed. in Wiley Series in Probability and Statistics. Wiley, 2006. doi: 10.1002/0470010940.
[28] S. Hekimoglu, B. Erdogan, M. Soycan, and U. M. Durdag, "Univariate Approach for Detecting Outliers in Geodetic Networks," *J. Surv. Eng.*, vol. 140, no. 2, p. 04014006, May 2014, doi: 10.1061/(ASCE)SU.1943-5428.0000123.
[29] H. Duman, "GNSS-specific characteristic signals in power spectra of multi-GNSS coordinate time series," *Adv. Space Res.*, vol. 73, no. 12, pp. 5860–5875, Jun. 2024, doi: 10.1016/j.asr.2024.03.016.
[30] P. Wessel *et al.*, "The Generic Mapping Tools Version 6," *Geochem. Geophys. Geosystems*, vol. 20, no. 11, pp. 5556–5564, Nov. 2019, doi: 10.1029/2019GC008515.